PHYSICAL REVIEW B VOLUME 58, NUMBER 2 1 JULY 1998-II

Correlation between domain structure and magnetoresistance in an active spin-valve element

X. Portier, E. Yu. Tsymbal, and A. K. Petford-Long
Department of Materials, University of Oxford, Oxford OX1 3PH, United Kingdom

T. C. Anthony and J. A. Brug
Hewlett-Packard Laboratories, 1501 Page Mill Road, Palo Alto, California 94304

(Received 18 March 1998)

In situ experiments in a Lorentz transmission-electron microscope have been performed on spin-valve elements through which a current is being applied. The ability to simultaneously measure the resistance and observe the domain structure of the element has allowed us to correlate magnetoresistance with the angle between the magnetization directions in the ferromagnetic layers. The angles have been obtained from summed image differential-phase-contrast images of the domains. A model is proposed to calculate the resulting magnetoresistance. The calculated data are in good agreement with the experimental magnetoresistance measured during observation of the magnetization reversal mechanism.
[S0163-1829(98)50526-7]

Numerous studies have been performed over the past few years on systems exhibiting giant magnetoresistance (Ref. 1, and references therein), mainly because of their potential use in information storage systems as magnetoresistive sensors or random access memory (MRAM) elements. Many of these devices involve spin-valve (SV) structures and considerable effort is still being expended to understand their behavior.[2] A SV consists of two ferromagnetic (FM) layers separated by a nonmagnetic material. The magnetization of one FM layer (pinned layer) is fixed by an adjacent antiferromagnetic layer (pinning layer) whereas the magnetization in the other FM layer (sense layer) is free to rotate, following the direction of an external applied magnetic field. Parallel (P) and anti-parallel (AP) alignments of the magnetizations of the pinned and sense layers correspond to the minimum and maximum resistance values of the film, respectively. Experimental studies[3,4] have shown that the resistivity of SV multilayers varies linearly with $\cos\theta$, where θ is the angle between the magnetization directions of the FM layers. A theoretical approach[5] has led to the same conclusion by considering a free-electron gas subjected to spin-dependent scattering at the interfaces or/and in the bulk of the layers. Calculations based on a realistic band structure of the Co/Cu/Co trilayers show just a slight deviation from the $\cos\theta$ dependence.[6]

The studies described above consider the average properties of magnetic films but it becomes necessary to study the local variations in properties, which will affect the behavior of devices whose size becomes smaller and smaller (less than 1 μm) and which can be studied by observation of the domain structure and local magnetization reversal mechanism. One of the most useful techniques for obtaining local magnetic information and correlating this with imperfections in the film structure is Lorentz transmission-electron microscopy (LTEM).[7] *In situ* magnetizing experiments have enabled magnetization reversal mechanisms to be studied at a local level, and more recently this technique has been applied to specially designed SV devices through which a current is applied *in situ* (i.e., active SV elements).[8] The study of active SV elements has provide a new tool for micromagnetic investigations; for example, a very recent study of a SV element submitted to various current values has clearly shown the effect of the thermal energy, as well as of the magnetic field induced by the sensing current,[9] on the reversal mechanism. Quantitative data on the magnetization distribution within the plane of the film can be extracted using the summed image differential phase contrast (SIDPC) technique—an implementation of LTEM based on Foucault imaging.[10] The purpose of the present work is to obtain quantitative SIDPC images of the domain structure of a SV element during reversal of the magnetization in the sense layer, and to calculate the resistance in the element, using computer modeling, from the contrast of the SIDPC images. These values are then compared with the experimental values of the resistance of the element measured using a two-point probe.

The *in situ* experiments performed in this study required fabrication of a lithographically-defined device, consisting of a 2 mm $\times$ 2 mm silicon substrate supporting a 40-nm-thick alumina window on which a 10 μm $\times$ 70 μm SV element has been deposited. The structure of the SV film is Ta/NiFe/Cu/Co/NiFe/MnNi/Ta (5/8/3/2/6/25/5 nm). A 70-Oe field defined the easy axis during deposition and a post-deposition vacuum anneal at a temperature in excess of 220 °C for several hours in a 1-kOe field established a suitable exchange coupling between pinning and pinned layers by increasing the density of MnNi grains with the tetragonal phase.[11] The thin Co film of the pinned layer has been introduced to enhance the magnetoresistive properties of the SV structure.[12] Au contacts deposited at each end of the SV result in an active element 10 μm $\times$ 30 μm in size sitting over an electron transparent alumina window. Details of the fabrication process are given elsewhere.[8]

In situ magnetizing experiments were carried out using a modified JEOL 4000EX TEM operated at 400 kV and fitted with an AMG40 low-field objective lens pole piece (residual field at the specimen position <1 Oe). A specimen holder, equipped with magnetizing coils, has been constructed in which the SV device is clamped by two Au-coated pads making electrical contacts between the device and an exter-

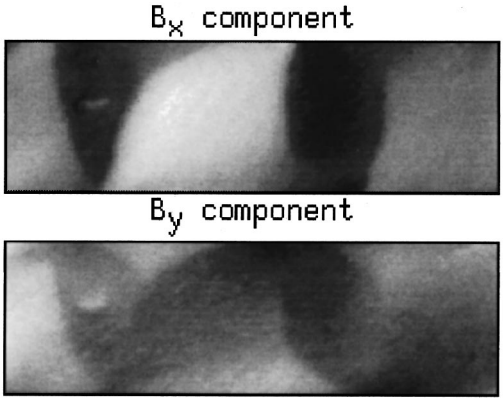

FIG. 1. SIDPC images showing the x and y components of the in-plane magnetization in the 10 μm $\times$ 30 μm SV element in an applied field of -10.26 Oe. The applied field as well as the x axis are parallel to the long axis of the element. The y axis is vertical.

nal electrical circuit providing controllable currents and reading of the voltage. By monitoring the change in voltage with change in applied field, the MR curve of the sample could be plotted. The applied field, parallel to the easy axis, was changed by 1 Oe every 10 s in order to keep constant any time-dependent effects. Quantitative maps of the in-plane magnetization of the SV element were obtained, with a spatial resolution of about 8 nm, using the SIDPC technique.[9] The two images in Fig. 1 show the x and y components of the in-plane magnetization of the SV element for an applied field of -10.26 Oe. Each 232×72 image is reduced to a 29×9 array with each pixel having the average value of an 8×8 pixel area of the original array. Each pixel now corresponds to a unit ~1 μm^2 of the element. The x and y components of the in-plane induction of each unit are proportional to the intensities of the corresponding pixels. An arrow map can then be produced with the magnitude and direction of the magnetization in each unit represented by an arrow of suitable length and direction. By collecting a series of SIDPC images for different applied magnetic field values, the magnetization reversal of the sense layer could be followed.

In the following sections, we will assume that the magnetization direction of the pinned layer remains constant and parallel to the easy axis. This assumption is based on the fact that the exchange-coupling produced in the NiFe/MnNi bilayer system is very high ($\sim$500 Oe), and the range of applied magnetic field used to plot the MR curves is $<\pm35$ Oe. Figure 2 shows a set of data recorded during the P-to-AP reversal of the sense layer magnetization. Figures 2(b), 2(d), 2(f), and 2(h) show scattergrams corresponding to the magnetization maps; all arrows in a map with the same direction and magnitude correspond to a single point in the scattergram. A similar series was recorded for the AP-to-P transition (not shown). Prior to observing each transition a saturating field up to ±400 Oe was applied. Each arrow in the vector maps represents the magnitude and direction of the total in-plane magnetization, $\mathbf{M}_T$, of the SV element in a 1 μm^2 area. Let the constant magnetization of the pinned layer be $\mathbf{M}_P$. Since the FM layers have the same thickness (8 nm), we can assume that the maximum magnetization, $\mathbf{M}_S$, of the sense layer has the same magnitude as $\mathbf{M}_P$ (i.e., $|\mathbf{M}_P|=|\mathbf{M}_S|=M$). Note however that the presence of a thin Co layer in the pinned layer, and imperfections in the exchange coupling between the pinning and pinned layers are expected to introduce a slight difference between $|\mathbf{M}_P|$ and $|\mathbf{M}_S|$. The total magnetization of the film for each unit is then $\mathbf{M}_P+\mathbf{M}_S$, and equals 0 for the AP state and $2M$ for the P state. The data in Fig. 2 clearly show the way in which the total magnetization of the SV element decreases from $2M$ to 0 as the sense layer magnetization switches from the P to the AP configuration. $\mathbf{M}_P$ is deduced from the P state and $\mathbf{M}_S$ equals $\mathbf{M}_T-\mathbf{M}_P$. Knowing $\mathbf{M}_P$ and $\mathbf{M}_S$ for a given applied field value, the angles between the sense and pinned layer magnetizations can be determined for each unit of the array defining the SV element.

In order to correlate the angular distributions with measured resistances we have developed a model for calculating the resistance. The model is based on the approximation that the dimensions of the array units are large with respect to the electronic mean-free path and therefore the local resistivity within a unit can be defined by the bulk value of the resistivity for the system. This approximation allows an equivalent circuit model to be used for calculating the resistance. This idea is well known in the conductivity theory of binary alloys (see, e.g., Ref. 13). In the SV films in this study the resistance of each unit depends on the angle θ between the magnetization of the two FM films. Following the results of Ref. 3–5 we assume that the resistance of a unit changes linearly with $\cos\theta$:

$$r_{ij}=\frac{1}{2}(r_{\mathrm{P}}+r_{\mathrm{AP}})+\frac{1}{2}(r_{\mathrm{P}}-r_{\mathrm{AP}})\cos\theta_{ij}. \tag{1}$$

Here indices i,j denote the unit, $i=1,\ldots n$, $j=1,\ldots m$, and n and m are the number of subdivisions in the two directions ($n=29$ and $m=9$); θ_{ij} is the angle between the magnetization directions for the (i,j) cell and r_{P} and r_{AP} are the resistance values of the unit for $\theta_{ij}=0$ and $\theta_{ij}=\pi$, respectively.

We note that within the equivalent circuit model it is not possible to subdivide the SV structure in the direction perpendicular to the layers, because the thicknesses of the layers are comparable to or less than the electronic mean-free path. Our model, therefore, makes no distinction between the interfacial and bulk scattering, both mechanisms of scattering being included in r_{ij}. We also assume that there is no transverse variation in the electron scattering properties of the SV element which is reflected in the fact that both r_{P} and r_{AP} in Eq. (1) are taken to be independent of a particular unit (i,j).

In order to calculate the net resistance of the system we converted the two-dimensional microstructure into a network of resistors by connecting each pair of adjacent units by a resistor as shown in Fig. 3. The conductance of the resistor between the nearest-neighbor units (i,j) and (k,l) is determined by the resistance r_{ij} and r_{kl} of the units and can be defined in two different ways:

$$\sigma_{ij,kl}=2(r_{ij}+r_{kl})^{-1} \tag{2}$$

for connection in series, and

$$\sigma_{ij,kl}=\frac{1}{2}(r_{ij}^{-1}+r_{lk}^{-1}) \tag{3}$$

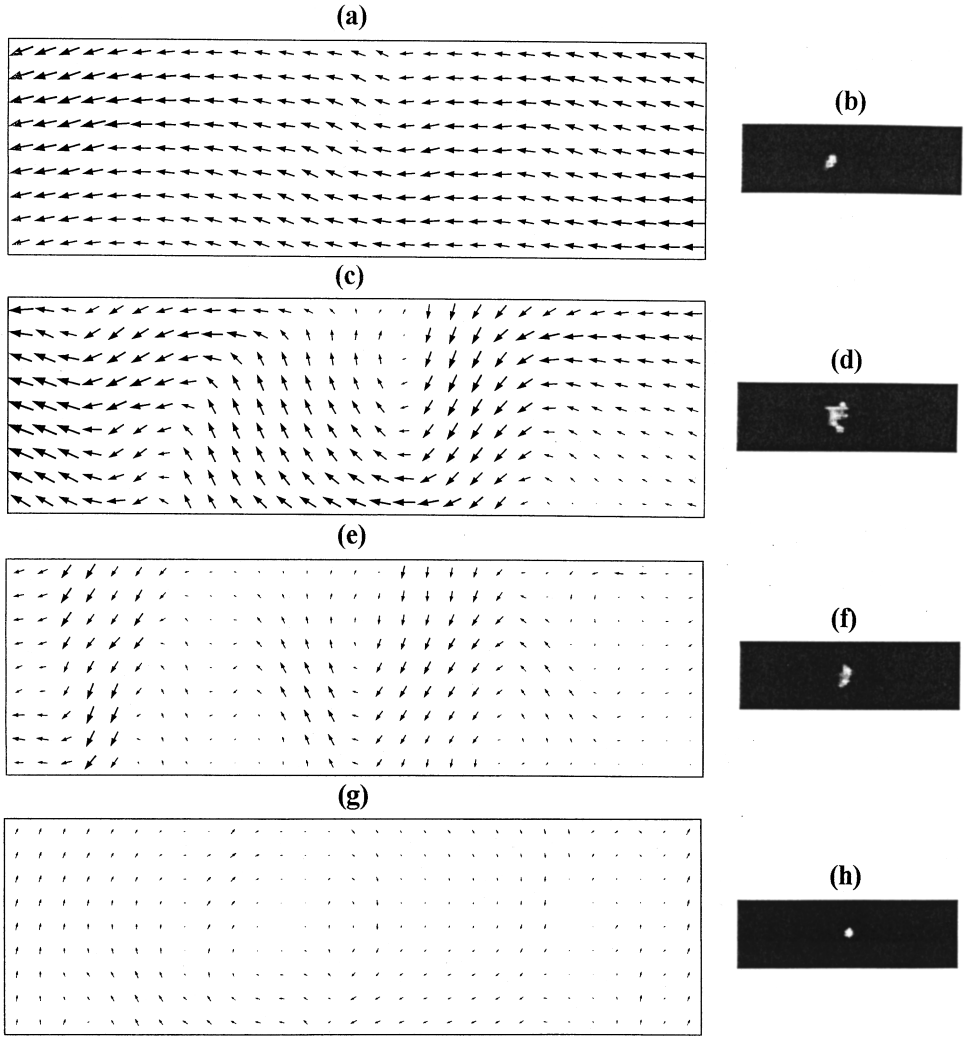

FIG. 2. Arrow maps and corresponding scattergrams of the magnetization distribution in the SV element during the P (total magnetization $2M$) to AP (total magnetization 0) reversal of the magnetization in the sense layer for applied fields of: (a) and (b) -0.76 Oe, (c) and (d) -10.26 Oe, (e) and (f) -15.30 Oe, and (g) and (h) -21.66 Oe. The data were obtained using the SIDPC technique.

for connection in parallel. We found, however, that the net resistance is almost independent of the choice of the connection type (2) or (3) which is not unusual because of the relatively small difference between r_{P} and r_{AP}.

The current conservation law for this network requires that

$$(\phi_{ij}-\phi_{i-1j})\sigma_{i-1j,ij}+(\phi_{ij}-\phi_{ij-1})\sigma_{ij-1,ij}$$

$$+(\phi_{ij}-\phi_{i+1j})\sigma_{ij,i+1j}+(\phi_{ij}-\phi_{ij+1})\sigma_{ij,ij+1}=0, \quad (4)$$

where ϕ_{ij} is the value of the potential at a node associated with the unit (i,j). This is a system of simultaneous equations for the value of the potential at each of the interior nodes. The potential on the left and right exterior nodes is determined by the boundary conditions:

$$\phi_{0j}=0, \quad \phi_{n+1j}=V; \quad j=1,...,m, \quad (5)$$

where V is the applied voltage. The boundary conditions for the conductance at the top and bottom nodes are

$$\sigma_{i0,i1}=0, \quad \sigma_{im,im+1}=0; \quad i=1,...,n. \quad (6)$$

The calculation of the net resistance was performed in two steps. First, we calculated the dimensionless resistance r_0 of the network assuming that all the resistances r_{ij} are equal to unity. This resistance served as a normalizing con-

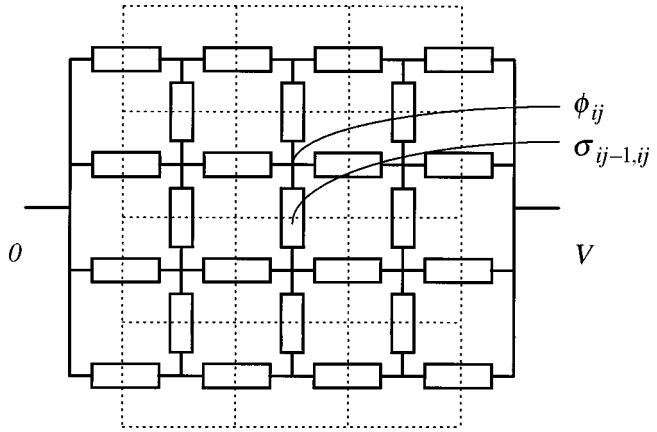

FIG. 3. A resistor network used for calculating the resistance. The dashed line shows schematically the array of units used for the magnetization orientation map.

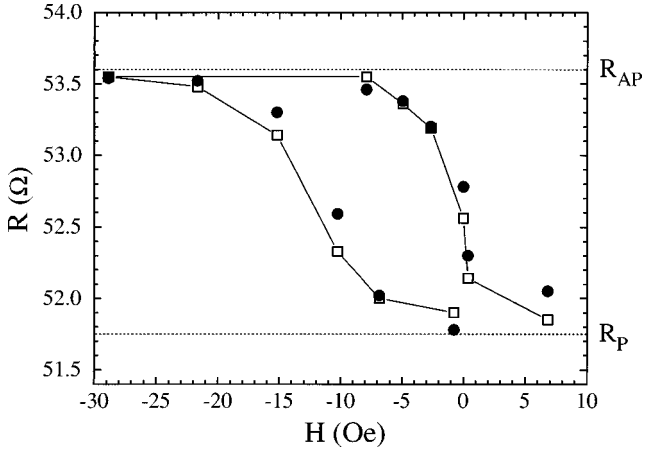

FIG. 4. Plots of the experimental (empty squares) and calculated (full circles) values of resistance versus applied field for reversal of the magnetization of the sense layer in the SV element. R_P and R_{AP} are the extremum values recorded for the P and AP alignments of the magnetic inductions, respectively. See text for explanations.

stant. Then, using the experimental values of the resistance for parallel and antiparallel configurations, R_P and R_{AP}, we determined r_P and r_{AP} in Eq. (1) from $r_P = R_P/r_0$ and $r_{AP} = R_{AP}/r_0$.

The resistance values r_{ij} were found using the array of angles θ_{ij} determined experimentally. Then, taking into account Eqs. (2) or (3) and Eqs. (5)–(6) and solving system (4) numerically, we determined the net resistance R of the complete SV element. Figure 4 shows plots of the resistance versus applied field for reversal of the magnetization of the sense layer in the SV element. The empty squares indicate the resistance values determined using the model described above, with the values of cos θ taken from the experimentally recorded SIDPC maps. R_P and R_{AP} are the extremum values recorded for the P and AP alignments of the magnetic induction, respectively. We stress that, since the values of R_P and R_{AP} are known from the experiment, the calculated hysteresis curve does *not* contain any adjustable parameters. As can be seen, the agreement between the two sets of data is good, indicating that the model that we have chosen to use is valid for this type of system.

In conclusion, we have successfully shown a correlation between the domain structure and magnetoresistance of a SV element by deducing the local resistance of small regions from the contrast of SIDPC images recorded during magnetization reversal of the sense layer, and using this as input to a computer model. The advantage of such an approach is that all the magnetostatic components due to FM coupling, shape anisotropy, or even field induced by the sensing current, are included in the observed domain structure and consequently can be taken into account in our model. Similar experiments on smaller elements are in progress. The proposed model for calculating the resistance can be used for simulating GMR curves in micromagnetic modeling.

This research has been supported by Hewlett-Packard Laboratories in Palo Alto through a collaboration with the Department of Materials in Oxford University. The calculations have been performed in the Materials Modeling Laboratory at the Department of Materials, Oxford University. The authors thank B. Garcia for his help in making the masks used for the lithographic procedure. X.P. is grateful to P. Bayle-Guillemaud for her expertise in using the Semper program. E.Y.T. is grateful to D.G. Pettifor for many discussions. A.K.P.L. wishes to thank the Royal Society for financial support.

[1] A. Fert and P. Bruno, in *Ultrathin Magnetic Structures II: An Introduction to the Electronic, Magnetic and Structural Properties,* edited by J. A. C. Bland and B. Heinrich (Springer-Verlag, Berlin, 1994).

[2] B. Dieny, J. Magn. Magn. Mater. **36**, 335 (1994).

[3] A. Chaiken, G. A. Printz, and J. J. Krebs, J. Appl. Phys. **67**, 4892 (1990).

[4] B. Dieny, V. S. Speriosu, S. S. P. Parkin, B. A. Gurney, D. R. Wilhoit, and D. Mauri, Phys. Rev. B **43**, 1297 (1991).

[5] S. Zhang, P. M. Levy and A. Fert, Phys. Rev. B **45**, 8689 (1992).

[6] R. H. Brown, D. M. C. Nicholson, W. H. Butler, X.-G. Zhang, W. A. Shelton, T. C. Schulthess, and J. M. MacLaren, J. Appl. Phys. **81**, 4008 (1997).

[7] J. P. Jakubovics, *Electron Microscopy in Materials Science,* edited by E. Ruedl and U. Valdre (Commission of the European Communities, Brussels and Luxembourg, 1975), Vol. IV, p. 1303.

[8] X. Portier, A. K. Petford-Long, R. C. Doole, J. A. Brug, and T. C. Anthony, IEEE Trans. Magn. **33**, 3574 (1997).

[9] X. Portier, A. K. Petford-Long, J. A. Brug, and T. C. Anthony (unpublished).

[10] A. C. Daykin and A. K. Petford-Long, Ultramicroscopy **58**, 365 (1995).

[11] X. Portier, A. K. Petford-Long, and T. C. Anthony, IEEE Trans. Magn. **33**, 3679 (1997).

[12] S. S. P. Parkin, Appl. Phys. Lett. **61**, 1358 (1992).

[13] A. P. Roberts and M. Teubner, Phys. Rev. E **51**, 4141 (1995).